

Output-Feedback Full-State Targeting Model Predictive Control for Station-Keeping on Near-Rectilinear Halo Orbits

Yuri Shimane¹, Stefano Di Cairano², Koki Ho³, and Avishai Weiss⁴

Abstract—We develop a model predictive control (MPC) policy for station-keeping (SK) on a Near-Rectilinear Halo Orbit (NRHO). The proposed policy achieves full-state tracking of a reference NRHO via a two-maneuver control horizon placed one revolution apart. Our method abides by the typical mission requirement that at most one maneuver is used for SK during each NRHO revolution. Simultaneously, the policy has sufficient controllability for full-state tracking, making it immune to phase deviation issues in the along-track direction of the reference NRHO, a common drawback of existing SK methods with a single maneuver per revolution. We report numerical simulations with a navigation filter to demonstrate the MPC’s performance with output feedback. Our approach successfully maintains the spacecraft’s motion in the vicinity of the reference in both space and phase, with tighter tracking than state-of-the-art SK methods and comparable delta-V performance.

I. INTRODUCTION

With growing interest in lunar exploration, libration point orbits (LPO) offer unique locations to place both robotic and crewed spacecraft. For example, the lunar Gateway is planned in the 9:2 resonant southern Near-Rectilinear Halo Orbit (NRHO) about the Earth-Moon L2 point [1]. The instability of LPOs necessitates station-keeping (SK) maneuvers, also referred to as orbit maintenance maneuvers (OMMs), to be conducted by the spacecraft. The purpose of SK is to maintain the spacecraft near a pre-computed reference LPO, or *baseline*, under the presence of uncertainties such as state estimation error, modeling error, and control execution error. Due to the stringent propellant budget, typically higher instability of LPOs compared to traditional orbits around planets and moons, and the low number of heritage missions flying on LPOs, SK techniques on LPOs are an active area of research.

To accommodate mission operations, SK maneuvers are typically required to be as infrequent as possible [2]. On the NRHO with an orbital period of about 6.55 days, a typical requirement is for SK maneuvers to be conducted at most once every revolution about the Moon. To adhere to this requirement, a commonly adopted approach is the *x-axis crossing control* [2], a shooting-based method for designing SK maneuvers. In the *x-axis crossing control*, a single 3-degrees-of-freedom (DOF) control maneuver is

designed at each revolution to target a subset of the spacecraft state at a perilune along the baseline a few revolutions downstream. Recently, the CAPSTONE mission [3] adopted this SK technique, and some variants are currently being studied for the upcoming Gateway mission [2].

One drawback of the *x-axis crossing control* stems from the fact that at most three out of the six translational state components can be assigned. To overcome this deficiency, *x-axis crossing control* leverages the LPO’s plane of symmetry. A subset of the predicted spacecraft state at the intersection with the plane of symmetry is matched with the corresponding state components along the baseline when it intersects the same plane. Using the plane of symmetry results in a discrepancy between the epoch when the spacecraft crosses the plane and when the baseline crosses the plane. As a result, the steered path may experience a phase angle disparity: the spacecraft’s position along the orbit may drift ahead or behind the baseline. To date, the phase disparity has been treated by ad-hoc heuristics, e.g. augmenting the targeting scheme with the epoch at which the symmetry event occurs [2], [4], or encapsulating the targeting scheme within a constrained optimization problem formulation [5]. For further details, see [6] and references therein.

Here, we propose a model predictive control (MPC) policy that overcomes the phase disparity via full-state targeting. The proposed MPC uses a control horizon with two maneuvers spaced one revolution apart, which provides sufficient controllability to track all six state components. Simultaneously, the one-revolution control cadence ensures our approach is consistent with the operational requirement of conducting up to a single SK maneuver per revolution. To minimize the propellant consumption explicitly, we employ an economic objective [7], [8] based solely on the control cost. The proposed MPC, hereafter denoted as SKMPC, sequentially solves a second-order cone program (SOCP) that steers the state of the spacecraft to the vicinity of the baseline at the end of its targeting horizon. At each iteration, the SOCP is re-instantiated by linearizing the dynamics about the steered state from the previous iteration; the SKMPC is terminated when the steered state propagated with the nonlinear dynamics lies sufficiently close to the baseline. We provide a brief discussion on the recursive feasibility of the SKMPC and numerically demonstrate its performance.

While other MPC-based approaches [9], [10], [11] also adopt a full-state tracking approach, they do not account for the requirement of a single maneuver per revolution. Our SKMPC meets this critical requirement, thus making it a promising approach for future missions.

^{1,3}Y. Shimane and K. Ho are with the Daniel Guggenheim School of Aerospace Engineering, Georgia Institute of Technology, Atlanta, GA 30332, USA Emails: {yuri.shimane, kokiho} at gatech.edu

^{2,4}S. Di Cairano and A. Weiss are with Mitsubishi Electric Research Laboratories (MERL), Cambridge, MA 02139, USA Emails: {dicairano, weiss} at merl.com

In this work, we extend [12] by augmenting a navigation filter to estimate the full state of the spacecraft, validating the proposed approach in a realistic output-feedback scenario. Our simulation incorporates disturbances due to navigational uncertainty, dynamics modeling errors, control actuation errors, and random impulses imparted at scheduled times along the NRHO due to momentum wheel desaturation maneuvers. We provide comprehensive Monte Carlo results with varying disturbance levels, thereby quantifying the coupled performance of the filter and the SKMPC.

II. BACKGROUND

First, we model the spacecraft dynamics, and then provide a brief introduction to LPOs and their stability.

A. Spacecraft Dynamics Model

We consider the spacecraft's motion in the inertial frame \mathcal{F}_{Inr} , centered at the Moon. The state of the spacecraft $\mathbf{x} \in \mathbb{R}^6$ consists of the Cartesian position $\mathbf{r} \in \mathbb{R}^3$ with respect to the Moon and the rate of change of \mathbf{r} in \mathcal{F}_{Inr} , denoted by $\mathbf{v} \in \mathbb{R}^3$. The equations of motion are given by [13]

$$\dot{\mathbf{x}} = \mathbf{f}[\mathbf{x}(t), t] = \begin{bmatrix} \mathbf{v} \\ -\frac{\mu}{r^3}\mathbf{r} + \mathbf{a}_{\text{J2}} + \sum_i \mathbf{a}_{N_i} + \mathbf{a}_{\text{SRP}} \end{bmatrix}, \quad (1)$$

where $r = \|\mathbf{r}\|_2$, and μ is the gravitational parameter of the Moon. The derivative of \mathbf{v} consists, in order, of the Keplerian acceleration due to the Moon, J2 perturbation of the Moon \mathbf{a}_{J2} , gravitational perturbations by other celestial bodies \mathbf{a}_{N_i} , and the solar radiation pressure (SRP) \mathbf{a}_{SRP} . These terms are given by

$$\mathbf{a}_{\text{J2}} = \mathbf{T}_{\text{Inr}}^{\text{PA}} \left(-\frac{3\mu J_2 R_{\text{Moon}}^2}{2r^5} \begin{bmatrix} \left(1 - 5\frac{z_{\text{PA}}^2}{r^2}\right) x_{\text{PA}} \\ \left(1 - 5\frac{z_{\text{PA}}^2}{r^2}\right) y_{\text{PA}} \\ \left(3 - 5\frac{z_{\text{PA}}^2}{r^2}\right) z_{\text{PA}} \end{bmatrix} \right), \quad (2a)$$

$$\mathbf{a}_{N_i} = -\mu_i \left(\frac{\mathbf{r}_i}{r_i^3} + \frac{\mathbf{d}_i}{d_i^3} \right), \quad (2b)$$

$$\mathbf{a}_{\text{SRP}} = P_{\text{Sun}} \left(\frac{\|\mathbf{d}_{\text{Earth}} - \mathbf{d}_{\text{Sun}}\|_2}{r_{\text{Sun}}} \right)^2 C_r \frac{A}{m} \frac{\mathbf{r}_{\text{Sun}}}{r_{\text{Sun}}}, \quad (2c)$$

respectively, where J_2 is the coefficient due to the oblateness of the Moon, R_{Moon} is the equatorial radius of the Moon, where $[x_{\text{PA}}, y_{\text{PA}}, z_{\text{PA}}]$ is the position vector components of the spacecraft resolved in the Moon's principal axes frame \mathcal{F}_{PA} , $\mathbf{T}_{\text{Inr}}^{\text{PA}} \in \mathbb{R}^{3 \times 3}$ is the transformation matrix from \mathcal{F}_{PA} to \mathcal{F}_{Inr} , μ_i is the gravitational parameter of body i , \mathbf{d}_i is the position of body i with respect to the Moon, $d_i = \|\mathbf{d}_i\|_2$, $\mathbf{r}_i = \mathbf{r} - \mathbf{d}_i$ is the position of the spacecraft with respect to body i in \mathcal{F}_{Inr} , $r_i = \|\mathbf{r}_i\|_2$, P_{Sun} is the SRP magnitude at the 1 astronomical unit, C_r is the radiation pressure coefficient, and A/m is the pressure area-to-mass ratio of the spacecraft. We include third-body perturbations due to the Earth and the Sun. Note that \mathbf{a}_{J2} , \mathbf{a}_{N_i} and \mathbf{a}_{SRP} in equation (1) are time-dependent, making \mathbf{f} non-autonomous. Constants in the equations of motion and ephemerides of celestial bodies are taken from the SPICE toolkit [14].

An initial linear perturbation $\delta\mathbf{x}(t_0)$ can be linearly propagated to time t , denoted by $\delta\mathbf{x}(t)$, via the linear state-transition matrix (STM) $\Phi(t, t_0) \in \mathbb{R}^6$,

$$\delta\mathbf{x}(t) = \Phi(t, t_0)\delta\mathbf{x}(t_0). \quad (3)$$

The Jacobian of the dynamics may be used to construct the STM by solving the matrix initial value problem (IVP)

$$\begin{aligned} \dot{\Phi}(t, t_0) &= \frac{\partial \mathbf{f}(\mathbf{x}, t)}{\partial \mathbf{x}} \Phi(t, t_0), \\ \Phi(t_0, t_0) &= \mathbf{I}_n. \end{aligned} \quad (4)$$

We use the shorthand notations $\mathbf{x}_j = \mathbf{x}(t_j)$ and $\Phi_{j,i} = \Phi(t_j, t_i)$, and we express the block submatrices of $\Phi_{j,i}$ as

$$\Phi_{j,i} = \begin{bmatrix} \Phi_{j,i}^{rr} & \Phi_{j,i}^{rv} \\ \Phi_{j,i}^{vr} & \Phi_{j,i}^{vv} \end{bmatrix}. \quad (5)$$

Assuming impulsive thrust¹ is available to control the spacecraft state, the state at time t_{k+1} with an impulse applied at time t_k is given by

$$\mathbf{x}_{k+1} = \mathbf{x}_k + \int_{t_k}^{t_{k+1}} \mathbf{f}[\mathbf{x}(t), t] + \delta(t - t_k) \begin{bmatrix} \mathbf{0}_{3 \times 1} \\ \mathbf{u}_k \end{bmatrix} dt, \quad (6)$$

where the control $\mathbf{u}_k \in \mathbb{R}^3$ is an impulsive change in velocity and δ is the Dirac delta function. Assuming $\|\mathbf{u}_k\|$ is much smaller compared to the dominant forces in (1), we can linearly approximate (6) as

$$\mathbf{x}_{k+1} = \mathbf{x}_k + \int_{t_k}^{t_{k+1}} \mathbf{f}[\mathbf{x}(t), t] dt + \begin{bmatrix} \Phi_{k+1,k}^{rv} \\ \Phi_{k+1,k}^{vv} \end{bmatrix} \mathbf{u}_k. \quad (7)$$

To facilitate the formulation of the SKMPC, we define the Earth-Moon rotating frame, \mathcal{F}_{EM} , with its x -axis aligned with the Earth-Moon vector, z -axis aligned with the co-rotating angular velocity vector of the Earth and the Moon, and the y -axis completing the triad. Note that due to the co-orbital motion of the Earth and the Moon, \mathcal{F}_{EM} is dynamic.

B. Canonical Scales

The large discrepancy in magnitude between \mathbf{r} components expressed in km and \mathbf{v} components expressed in km/s causes the STM to have poor numerical conditioning. To alleviate this effect, the dynamics from equation (1) can be resolved in terms of canonical scales, where \mathbf{r} is in terms of some length unit LU, and \mathbf{v} is in terms of some velocity unit VU. We choose LU = 100 000 km and define VU $\triangleq \sqrt{\mu/\text{LU}}$. The canonical time unit TU simply follows as TU = LU/VU. Once LU, TU, and VU are defined, all dynamical coefficients in equation (1) are re-scaled accordingly. Further detail on how to choose LU is provided in [12].

¹Due to control executions lasting on the order of seconds to minutes along an orbit with a period on the order of days, all conventional thrusters are effectively impulsive in this application.

C. Libration Point Orbits

Libration point orbits (LPOs) are bounded motions revolving around libration points of the three-body system such as the Earth-Moon-spacecraft system. While periodic LPOs can only exist in simplified dynamics models such as the restricted three-body problems, quasi-periodic motion still exists in the full-ephemeris dynamics model (1). LPOs occupy spatial regions and energy levels that may not be covered by “traditional” orbital motions revolving around planetary bodies, thus providing mission designers attractive alternative spacecraft destinations. For example, the southern NRHO about the Earth-Moon L2 has been selected as the location for the Lunar Gateway, a planned crew station in cislunar space [15]. In this work, we use the 15-year-long baseline NRHO from NASA [1].

D. Stability on Near Rectilinear Halo Orbit

Many LPOs, including the NRHO, possess both stable and unstable subspaces. The unstable subspace on LPOs necessitates station-keeping actions to prevent the spacecraft from diverging from the baseline, especially when considering uncertainties in navigation and thrust actuation.

To quantify the local instability along the NRHO, we evaluate the 1-revolution finite-time Lyapunov exponent (FTLE)

$$\text{FTLE} = \frac{1}{|T|} \ln \sqrt{\lambda_{\max}(\Phi_{t_0+T, t_0})}, \quad (8)$$

where $T \approx 6.55$ days is the approximate orbital period of the NRHO, and $\lambda_{\max}(\Phi_{t_0+T, t_0})$ is the largest eigenvalue of Φ_{t_0+T, t_0} . Figure 1 shows the FTLE evaluated at various locations along the NRHO. We introduce the *osculating true anomaly* θ to facilitate the discussion about the varying stability along the NRHO. Following the Keplerian definition for a spacecraft orbiting the Moon,

$$\theta = \text{atan2}(hv_r, h^2/r - \mu), \quad (9)$$

where $h = \|\mathbf{h}\|_2 = \|\mathbf{r} \times \mathbf{v}\|_2$ is the angular momentum, and $v_r = \mathbf{r} \cdot \mathbf{v}/r$ is the radial velocity. It is apparent from Figure 1 that the dynamics are most sensitive at *perilune* where $\theta = 0^\circ$ and the spacecraft is closest to the Moon, and least sensitive at *apolune* where $\theta = 180^\circ$. For further details on the dynamics in NRHO, see [15] and references therein.

To make the SK activity as robust as possible against navigation and control actuation errors, SK maneuvers typically execute near apolune. Let the *maneuver true anomaly* θ_{man} denote the osculating true anomaly where the SK maneuver is scheduled to occur. In accordance with operational plans for the Gateway [2], we use $\theta_{\text{man}} = 200^\circ$. We also choose to target the baseline at an apolune N revolutions downstream to minimize the targeting sensitivity. In summary, the controller proposed in this work aims to design an SK maneuver at θ_{man} such that the steered state lies in the vicinity of the baseline at the N^{th} apolune into the future, i.e., approximately N revolutions later.

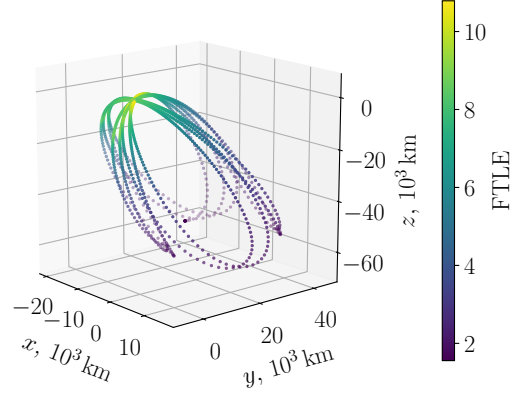


Fig. 1: NRHO state history in Moon-centered J2000 frame

E. Navigation Filter

We consider an extended Kalman filter (EKF) to estimate the spacecraft state. Let $\hat{\mathbf{x}} \in \mathbb{R}^6$ and $\mathbf{P} \in \mathbb{R}^{6 \times 6}$ denote the state and covariance estimates of the filter, respectively. We briefly present the prediction and update steps of the EKF, along with the measurement model and the impulse events.

1) *Prediction*: The prediction step from time t_{k-1} to t_k is given by

$$\begin{aligned} \hat{\mathbf{x}}_{k|k-1} &= \hat{\mathbf{x}}_{k-1|k-1} + \int_{t_{k-1}}^{t_k} \mathbf{f}[\hat{\mathbf{x}}(t), t] dt, \\ \mathbf{P}_{k|k-1} &= \Phi_{k,k-1} \mathbf{P}_{k-1|k-1} \Phi_{k,k-1}^T + \mathbf{Q}_{k,k-1}, \end{aligned}$$

where $\mathbf{Q}_{k,k-1}$ is the process noise accounting for unmodelled disturbances. We adopt the unbiased random process noise model [16]

$$\mathbf{Q}_{k,k-1} = \sigma_p^2 \begin{bmatrix} (\Delta t^3/3) \mathbf{I}_3 & (\Delta t^2/2) \mathbf{I}_3 \\ (\Delta t^2/2) \mathbf{I}_3 & \Delta t \mathbf{I}_3 \end{bmatrix},$$

where σ_p is a tuning parameter.

2) *Update*: At time t_k , a measurement is provided to the filter. The noisy measurement $\mathbf{y}_k \in \mathbb{R}^m$ is assumed to follow a multivariate normal distribution with zero mean and covariance \mathbf{R}_k such that

$$\mathbf{y}_k = \mathbf{h}[\mathbf{x}(t_k)] + \mathcal{N}(\mathbf{0}_{m \times 1}, \mathbf{R}_k).$$

Let $\mathbf{H}_k = \partial \mathbf{h}[\mathbf{x}(t_k)] / \partial \mathbf{x}(t_k)$, the update step is

$$\begin{aligned} \mathbf{L}_k &= \mathbf{P}_{k|k-1} \mathbf{H}_k^T \left(\mathbf{H}_k \mathbf{P}_{k|k-1} \mathbf{H}_k^T + \mathbf{R}_k \right)^{-1}, \\ \hat{\mathbf{x}}_{k|k} &= \hat{\mathbf{x}}_{k|k-1} + \mathbf{L}_k (\mathbf{y}_k - \mathbf{h}_k[\mathbf{x}_{k|k-1}]), \\ \mathbf{P}_{k|k} &= (\mathbf{I}_6 - \mathbf{L}_k \mathbf{H}_k) \mathbf{P}_{k|k-1} (\mathbf{I}_6 - \mathbf{L}_k \mathbf{H}_k)^T + \mathbf{L}_k \mathbf{R}_k \mathbf{L}_k^T. \end{aligned}$$

3) *Measurements*: We consider measurements based on range and range-rate. The corresponding measurement model and partials are

$$\begin{aligned} \mathbf{h}(\mathbf{x}) &= \begin{bmatrix} r \\ \dot{r} \end{bmatrix} = \begin{bmatrix} \|\mathbf{r}\|_2 \\ \mathbf{r}^T \mathbf{v} / \|\mathbf{r}\|_2 \end{bmatrix}, \\ \mathbf{H}(\mathbf{x}) &= \begin{bmatrix} \frac{x}{r} & \frac{y}{r} & \frac{z}{r} & 0 & 0 & 0 \\ v_x - \frac{x\dot{r}}{r} & v_y - \frac{y\dot{r}}{r} & v_z - \frac{z\dot{r}}{r} & \frac{x}{r} & \frac{y}{r} & \frac{z}{r} \end{bmatrix}. \end{aligned}$$

We assume a constant measurement covariance $\mathbf{R}_k = \mathbf{R} = \text{diag}(\sigma_r^2, \sigma_{\dot{r}}^2)$ where σ_r and $\sigma_{\dot{r}}$ are the standard deviations of the range and range-rate measurements.

4) *Impulse Events*: We model SK maneuvers as resulting in a velocity impulse on the spacecraft $\Delta \mathbf{v}_k = \Delta \hat{\mathbf{v}}_k + \mathcal{N}(\mathbf{0}_{3 \times 1}, \mathbf{V}_k)$, where $\Delta \hat{\mathbf{v}}$ is the expected impulse, and \mathbf{V}_k is the corresponding covariance. The maneuver estimate $\Delta \hat{\mathbf{v}}$ is computed by the SKMPC and $\mathbf{V}_k = (\sigma_{\Delta \mathbf{v}, \text{abs}} + \sigma_{\Delta \mathbf{v}, \text{rel}} \|\Delta \hat{\mathbf{v}}\|_2)^2 \mathbf{I}_3$, where $\sigma_{\Delta \mathbf{v}, \text{abs}}$ and $\sigma_{\Delta \mathbf{v}, \text{rel}}$ are the absolute and relative standard deviation of the thruster. Then, the state and covariance estimates are updated via

$$\begin{aligned} \hat{\mathbf{x}}_{k|k} &= \hat{\mathbf{x}}_{k|k-1} + \begin{bmatrix} \mathbf{0}_{3 \times 1} \\ \Delta \hat{\mathbf{v}}_k \end{bmatrix}, \\ \mathbf{P}_{k|k} &= \mathbf{P}_{k|k-1} + \begin{bmatrix} \mathbf{0}_{3 \times 3} & \mathbf{0}_{3 \times 3} \\ \mathbf{0}_{3 \times 3} & \mathbf{V}_k \end{bmatrix}. \end{aligned}$$

III. FULL-STATE TARGETING MPC FOR STATION-KEEPING ON NRHO

The SKMPC computes an SK maneuver based on the state estimate $\hat{\mathbf{x}}(t_0)$ at the current time t_0 from the EKF and a predicted future state $\hat{\mathbf{x}}(t_N)$ at some future target time $t_N > t_0$. In the remainder of this section, we omit the (\cdot) notation from estimated state quantities within the SKMPC.

A. Problem Formulation

Let \mathcal{U} denote the admissible control set, N denote the number of revolutions until the targeted apolune along the baseline, which occurs at some future time t_N , and $\mathcal{X}(t_N)$ denote the terminal constraint set at time t_N . We consider a control horizon with $2 \leq K \leq N$ impulsive maneuvers, denoted by $\mathbf{u}_k \in \mathbb{R}^3$ for $k = 0, \dots, K-1$. The maneuvers are placed at the K earliest instances in time t_k where $\theta(t_k) = \theta_{\text{man}}$ between the time when the controller is invoked, denoted by t_{invoked} , and t_N . Thus, for a maneuver time t_k , $k = 0, \dots, K-1$,

$$\begin{cases} t_k \geq t_{\text{invoked}} & k = 0 \\ t_k > t_{k-1} & k > 0 \end{cases} \text{ and } \theta(t_k) = \theta_{\text{man}}. \quad (14)$$

Without loss of generality, we hereafter assume that the controller is invoked when $\theta(t_{\text{invoked}}) = \theta_{\text{man}}$, such that $t_0 = t_{\text{invoked}}$. The maneuvers are used to steer the propagated state at t_N to reside in $\mathcal{X}(t_N)$. We formulate a minimization problem with an economic sum-of-2-norm objective of the K maneuvers, which corresponds directly to the propellant mass consumed via Tsiolkovsky's rocket equation [13]. The finite-horizon discrete-time OCP of the SKMPC is

$$\min_{\mathbf{u}_0, \dots, \mathbf{u}_{K-1}} \sum_{k=0}^{K-1} \|\mathbf{u}_k\|_2 \quad (15a)$$

$$\text{s.t. } \mathbf{x}_0^N + \sum_{k=0}^{K-1} \begin{bmatrix} \Phi_{N,k}^{rv} \\ \Phi_{N,k}^{vv} \end{bmatrix} \mathbf{u}_k \in \mathcal{X}(t_N), \quad (15b)$$

$$\mathbf{u}_k \in \mathcal{U}, \quad \forall k = 0, \dots, K-1. \quad (15c)$$

where $\mathbf{x}_0^N \triangleq \text{vec}(\mathbf{r}_0^N, \mathbf{v}_0^N)$ denotes the initial state propagated until the end of the prediction horizon,

$$\mathbf{x}_0^N = \begin{bmatrix} \mathbf{r}_0^N \\ \mathbf{v}_0^N \end{bmatrix} = \mathbf{x}_0 + \int_{t_0}^{t_N} \mathbf{f}[\mathbf{x}(t), t] dt, \quad (16)$$

and \mathbf{x}_0 is the state at t_0 . The STM submatrices $\Phi_{N,k}^{rv}$ and $\Phi_{N,k}^{vv}$ are constructed by linearizing about the free drift trajectory obtained by integrating (16). Linearizing about the free drift trajectory is akin to the EKF, as opposed to linearizing about the baseline path, which is akin to the linearized Kalman filter. The former results in a more accurate linearized model, since the free drift trajectory is closer to the desired controlled trajectory than the baseline.

The linearized dynamics in (15b) implies that the control action \mathbf{u}_k shifts the state within some trust-region $\delta \in \mathbb{R}^6$,

$$\|\mathbf{x}_0^N - (\mathbf{F}_u[\mathbf{x}_0, \mathbf{u}_0, \dots, \mathbf{u}_{K-1}])\| \leq \delta, \quad (17)$$

where \mathbf{F}_u integrates the nonlinear dynamics (6) from t_0 to t_N with controls $\mathbf{u}_0, \dots, \mathbf{u}_{K-1}$ provided in the argument,

$$\mathbf{F}_u = \mathbf{x}_0 + \int_{t_0}^{t_N} \mathbf{f}[\mathbf{x}(t), t] + \sum_{k=0}^{K-1} \delta(t - t_k) \begin{bmatrix} \mathbf{0}_{3 \times 1} \\ \mathbf{u}_k \end{bmatrix} dt. \quad (18)$$

In (15c), \mathcal{U} is the set of controls upper-bounded by a maximum executable control magnitude u_{max} ,

$$\mathcal{U} = \{\mathbf{u} \in \mathbb{R}^3 : \|\mathbf{u}\|_2 \leq u_{\text{max}}\}. \quad (19)$$

B. Definition of Terminal Constraint Set

We construct $\mathcal{X}(t_N)$ as a 6D ellipsoid centered at the baseline state at t_N , $\mathbf{x}_{N,\text{ref}} \triangleq [\mathbf{r}_{N,\text{ref}}^T, \mathbf{v}_{N,\text{ref}}^T]^T$,

$$\begin{aligned} \mathcal{X}(t_N) = \\ \{\mathbf{x} \in \mathbb{R}^6 : \|\mathbf{r} - \mathbf{r}_{N,\text{ref}}\|_2 \leq \epsilon_r, \|\mathbf{v} - \mathbf{v}_{N,\text{ref}}\|_2 \leq \epsilon_v\}, \end{aligned} \quad (20)$$

where ϵ_r and ϵ_v are the magnitude of the apses of the ellipsoid along position and velocity components and are tuning parameters. The terminal constraint (15b) can be replaced by two second-order cone (SOC) constraints,

$$\left\| \sum_{k=0}^{K-1} \Phi_{N,k}^{rv} \mathbf{u}_k + \mathbf{r}_0^N - \mathbf{r}_{N,\text{ref}} \right\|_2 \leq \epsilon_r, \quad (21a)$$

$$\left\| \sum_{k=0}^{K-1} \Phi_{N,k}^{vv} \mathbf{u}_k + \mathbf{v}_0^N - \mathbf{v}_{N,\text{ref}} \right\|_2 \leq \epsilon_v. \quad (21b)$$

Note that ϵ_r and ϵ_v are easier to tune in the \mathcal{F}_{EM} frame due to the near-invariance of the apolune state of the NRHO in this frame. Thus we enforce (21) with $\Phi_{N,k}^{rv}$, $\Phi_{N,k}^{vv}$, \mathbf{r}_0^N , and $\mathbf{r}_{N,\text{ref}}$ realized in \mathcal{F}_{EM} .

C. Recursive Feasibility

Next, we briefly discuss the recursive feasibility of problem (15) with input constraint (19) and terminal set constraint (20). The non-autonomous dynamics (1) results in the terminal set $\mathcal{X}(t_j)$ to also be time-dependent, complicating the application of the classical approach for proving recursive feasibility of MPC. Computing and storing such a time-varying set for the NRHO, which is not periodic but only

quasi-periodic, may be prohibitive in practice. However, this specific application has some favorable conditions that help us recover guarantees of recursive feasibility. First, for the considered family of orbits, the STM in (7) ensures controllability of the linearized system around the nominal orbit, described by $\mathbf{f}[\mathbf{x}_k, t]$. Second, the available thrust upper-bounded by u_{\max} is “significantly larger” than what is required in SK maneuvers, although the general desire is to minimize the requested thrust.

Proposition 1: Let $K \geq 2$ correspond to the number of maneuvers such that

$$\text{rank} \left(\begin{bmatrix} \left[\begin{smallmatrix} \Phi_{j+N,j}^{rv} \\ \Phi_{j+N,j}^{vv} \end{smallmatrix} \right] \cdots \left[\begin{smallmatrix} \Phi_{j+N,j+K-1}^{rv} \\ \Phi_{j+N,j+K-1}^{vv} \end{smallmatrix} \right] \end{bmatrix} \right) = 6, \quad \forall j = 0, 1, \dots$$

For a large enough u_{\max} , if (15) is feasible at time t_{j-1} then it is feasible at t_j . Furthermore, the trajectory remains bounded in a set \mathcal{X}_{bnd} at the apolune times t_j .

Proof. Since (15) is feasible at t_{j-1} , there exists $U_K(t_{j-1}) = [\mathbf{u}(t_{j-1}) \dots \mathbf{u}(t_{j+K-2})]$ such that $\mathbf{x}(t_{j-1+N}) \in \mathcal{X}(t_{j-1+N})$, and $\mathbf{x}(t_j)$ is obtained by applying $\mathbf{u}(t_{j-1})$ to (7). Let $\tilde{\mathbf{x}}(t_{j+N}) = \int_{t_{j-1+N}}^{t_{j+N}} \mathbf{f}[\mathbf{x}(t_{j-1+N}), t] dt$, where $\mathbf{x}(t_{j-1+N})$ is obtained by applying the entire sequence $U_K(t_{j-1})$ followed by open loop evolution. We need to prove that it is possible to obtain a state perturbation $\delta \mathbf{x}$ such that $\tilde{\mathbf{x}}(t_{j+N}) + \delta \mathbf{x} \in \mathcal{X}(t_{j+N})$.

Consider the candidate control sequence $U_K(t_j) = [\mathbf{u}(t_j) + \delta \mathbf{u}(t_j), \dots, \mathbf{u}(t_{j+K-1}) + \delta \mathbf{u}(t_{j+K-1}), \mathbf{u}(t_{j+K})]$ and

$$\tilde{\mathbf{x}}(t_{j+N}) = \begin{bmatrix} \Phi_{j+N,j+K}^{rv} \\ \Phi_{j+N,j+K}^{vv} \end{bmatrix} \mathbf{u}_{j+K} + \sum_{k=j+1}^{j+K-1} \begin{bmatrix} \Phi_{j+N,k}^{rv} \\ \Phi_{j+N,k}^{vv} \end{bmatrix} \delta \mathbf{u}_k.$$

Then, $\mathbf{x}(t_{j+N}) = \tilde{\mathbf{x}}(t_{j+N}) + \delta \mathbf{x} \in \mathcal{X}(t_{j+N})$ is guaranteed by the controllability in K steps for some $\Delta U_K(t_j) = [\delta \mathbf{u}(t_j), \dots, \delta \mathbf{u}(t_{j+K-1}), \mathbf{u}(t_{j+K})]$ which perturbs and extends the previous control sequence $U_K(t_{j-1})$. For a large enough u_{\max} , the sequence $U_K(t_j)$ is feasible. Due to the finite horizon and the bounded thrust, the trajectories remain bounded in a set \mathcal{X}_{bnd} because the control strategy enforces (15b), and using (20), $\mathcal{X}(t)$ is bounded by its definition. ■

With regards to the assumptions in Proposition 1, due to the quasi-periodic nature of the orbit, the difference between $\mathcal{X}(t_{j-1+N})$ and $\mathcal{X}(t_{j+N})$ is usually small. The necessitated correction $\delta \mathbf{x}$ is thus relatively small compared to the control authority u_{\max} . Hence, the maximum thrust of the propulsion system will be sufficient to ensure the feasibility of the candidate control sequence. The rank condition is ensured by the controllability of the spacecraft in the NRHO orbit.

D. Sequential Linearization Scheme

To improve on the prediction error introduced by the linearization in (15b), we employ a sequential linearization scheme. Sequential linearization has been previously found to improve the recursive convergence of optimization-based SK algorithms [5], [17]. In essence, sequential linearization involves re-solving problem (15), each time re-linearizing

the dynamics about the steered trajectory obtained from the previous solution.

We recast (15) as an SOCP by introducing slack variables for the 2-norm of \mathbf{u}_k for $k = 0, \dots, K-1$ in the objective (15a), replacing (15b) by the SOC constraints (21), and using definition (19) for \mathcal{U} in constraint (15c).

At each iteration of the sequential linearization, we update \mathbf{x}_0^N , $\Phi_{N,k}^{rv}$ and $\Phi_{N,k}^{vv}$ for $k = 0, \dots, K-1$ by considering the controlled trajectory with controls computed from the previous iteration. Let $\mathbf{u}_0^{(i)}, \dots, \mathbf{u}_{K-1}^{(i)}$ denote the solution to problem (15) at the i^{th} iteration. On the next iteration, \mathbf{x}_0^N is obtained by

$$\mathbf{x}_0^N = \begin{bmatrix} \mathbf{r}_0^N \\ \mathbf{v}_0^N \end{bmatrix} = \mathbf{F}_u[\mathbf{x}_0, \mathbf{u}_{0,\text{prev}}^{(i)}, \dots, \mathbf{u}_{K-1,\text{prev}}^{(i)}], \quad (22)$$

instead of equation (16), where \mathbf{F}_u is given by (18); in (22), $\mathbf{u}_{k,\text{prev}}^{(i)}$ is the cumulative k^{th} control

$$\mathbf{u}_k^{(i)} = \begin{cases} \mathbf{0}_{3 \times 1}, & i = 0, \\ \sum_{j=0}^{i-1} \mathbf{u}_{k,\text{prev}}^{(j)}, & i > 0. \end{cases}$$

Furthermore, $\Phi_{N,k}^{rv}$ and $\Phi_{N,k}^{vv}$ are reconstructed by linearizing the nonlinear flow around (22).

Algorithm 1 summarizes the SKMPC algorithm with the sequential linearization scheme. At a given time instance t_0 , the algorithm requires as input the current state estimate $\hat{\mathbf{x}}(t_0)$ treated as \mathbf{x}_0 , targeted time t_N , terminal constraint set $\mathcal{X}(t_N)$, admissible control set \mathcal{U} , and the maximum number of iterations for linearization M . In algorithm 1, $\mathbf{U} = \text{vec}[\mathbf{u}_{0,\text{prev}}, \dots, \mathbf{u}_{K-1,\text{prev}}]$ is the vectorized cumulative controls computed from successive SOCP solves, and $\mathbf{U}^{(i)} = \text{vec}[\mathbf{u}_0^{(i)}, \dots, \mathbf{u}_{K-1}^{(i)}]$ is the solution to the SOCP at the i^{th} iteration. The algorithm makes use of the following functions:

- IVP solves the initial value problem by integrating equation (22) along with the STM, applying the impulsive controls $\mathbf{u}_0, \dots, \mathbf{u}_{K-1}$ at times t_0, \dots, t_{K-1} .
- SOCP solves problem (15) recast into an SOCP by convex solvers such as ECOS [18] or SCS [19].

The algorithm terminates once the nonlinear steered state \mathbf{x}_0^N from (22) lies in $\mathcal{X}(t_N)$ and returns the earliest control $\mathbf{u}(t_0) = \mathbf{u}_0$, which is executed. Then, the spacecraft remains in the corrected orbit until the next maneuver instance t_1 , at which time Algorithm 1 is called again with updated time indices, sliding the targeting horizon t_N by one revolution, and a new sequence of controls is obtained.

IV. EXPERIMENT SETUP

The SKMPC is tested on a realistic SK scenario for a spacecraft flying on the NRHO. The simulation consists of recursively applying Algorithm 1 for an extended number of revolutions spanning multiple years, subject to navigation error from the EKF as well as dynamics model error, control execution error, and random impulses due to momentum wheel desaturation maneuvers imparted at predefined locations. The latter three errors are realized based on predefined Gaussian distributions. Each time the spacecraft arrives at

Algorithm 1 Sequential SKMPC

Inputs: $t_0, t_N, \mathbf{x}_0, \mathcal{X}(t_N), \mathcal{U}, M$

```

1:  $\mathbf{U} \leftarrow \mathbf{0}_{3K \times 1}$ 
2: for  $i = 0, \dots, M - 1$  do
3:    $\mathbf{x}_0^N, \Phi_{N,0}, \dots, \Phi_{N,K-1} \leftarrow \text{IVP}(t_0, t_N, \mathbf{x}_0, \mathbf{U})$ 
4:   if  $\mathbf{x}_0^N \in \mathcal{X}(t_N)$  then
5:     break
6:   end if
7:    $\mathbf{U}^{(i)} \leftarrow \text{SOCP}(\mathcal{X}(t_N), \mathcal{U}, \mathbf{x}_0^N, \Phi_{N,0}, \dots, \Phi_{N,K-1})$ 
8:    $\mathbf{U} \leftarrow \mathbf{U} + \mathbf{U}^{(i)}$ 
9: end for
10:  $\mathbf{u}_0 \leftarrow \mathbf{U}_{[0:3]}$ 

```

Outputs: \mathbf{u}_0

$\theta(t) = 200^\circ$, we denote t as t_0 , and Algorithm 1 is invoked using a control horizon defined by (14) with $\theta_{\text{man}} = 200^\circ$.

A. Error Models

The simulation involves repeatedly applying the EKF and executing an SK control every time the spacecraft reaches $\theta(t) = \theta_{\text{man}}$. The filter is initialized assuming an initial covariance $\mathbf{P}_{0|0} = \text{diag}([\sigma_{r_0}^2, \sigma_{r_0}^2, \sigma_{r_0}^2, \sigma_{v_0}^2, \sigma_{v_0}^2, \sigma_{v_0}^2])$ and an initial state estimate

$$\hat{\mathbf{x}}_{0|0} = \mathbf{x}(t_{\text{init}}) + \mathcal{N}(\mathbf{0}_{6 \times 1}, \mathbf{P}_{0|0}),$$

where $\mathbf{x}(t_{\text{init}})$ is the true state at the initial epoch t_{init} . At each revolution, when the spacecraft arrives at θ_{man} , a maneuver is computed using the state estimate of the filter, $\hat{\mathbf{x}}$, as \mathbf{x}_0 in Algorithm 1. The true state of the spacecraft is imparted with a corrupted maneuver using the Gates model [20]. In addition, we incorporate dynamics error, which consists of variation in SRP magnitude, and random impulses imparted by momentum wheel desaturation maneuvers [2]. The former is modeled by relative perturbations $\delta(A/m)$ and δC_r on A/m and C_r in (2c), and the latter is modeled by an additive velocity perturbation $\Delta \mathbf{v}$ with random direction and magnitude when the spacecraft arrives at $\theta(t) = \theta_{\text{desat}}$, where θ_{desat} are desaturation true anomalies dictated by mission requirements [2].

Table I summarizes the error parameters, corresponding to the assumed levels of uncertainties for the Gateway [21], along with the selected process noise parameter σ_p . Note that the choice of σ_p is dependent on the canonical scales in which the dynamics are expressed.

B. Navigation Update Model

In accordance with the typical operation of ground-based tracking, we assume measurements are provided during *tracking windows*, each lasting $\Delta t_{\text{track}} = 1$ hour. Let t_0 and $t_1 \approx t_0 + T$ denote two consecutive epochs where the maneuver is executed, such that $\theta(t_0) = \theta(t_1) = \theta_{\text{man}}$. In each revolution, there is one post-maneuver tracking window starting 12 hours after t_0 , and three pre-maneuver tracking windows, starting 72, 48, and 7 hours before t_1 . During each tracking window, we provide $N_{\text{meas}} = 10$ equally spaced measurements. Thus, at t_1 , Algorithm 1 uses the EKF's

TABLE I: Simulation parameters

Simulation parameter	Value
Average SRP A/m , m ² /kg	315/17900
Average SRP C_r	2
SRP rel. $\delta(A/m)$ 3- $\sigma_{A/m}$, %	30
SRP rel. δC_r 3- σ_{C_r} , %	15
Desaturation velocity magnitude 3- σ_{desat} , cm/s	1.0
Desaturation true anomaly θ_{desat} , deg	0° or 330°, 0° or 330°, 0°, 30°
Maneuver rel. magnitude error 3- $\sigma_{\Delta \mathbf{v}, \text{rel}}$, %	1.5
Maneuver abs. magnitude error 3- $\sigma_{\Delta \mathbf{v}, \text{abs}}$, mm/s	1.42
Maneuver execution direction error 3- $\sigma_{\Delta \mathbf{v}, \text{dir}}$, deg	1°
Initial position standard deviation 3- σ_{r_0} , km	10
Initial velocity standard deviation 3- σ_{v_0} , mm/s	10
Range measurement 3- σ_r , m	1
Range-rate measurement 3- $\sigma_{\dot{r}}$, mm/s	0.1
Process noise parameter σ_p	5×10^{-5}

predicted state estimate following the latest measurement update provided $t_1 - 7 + \Delta t_{\text{track}} = 6$ hours earlier.

C. Control Trigger Condition

To improve the delta-V performance of the SKMPC under navigation and execution errors, we consider a trigger condition to determine whether a maneuver is necessitated. The condition checks if the unsteered state predicted until t_N lies within an ellipsoid about the baseline with radii $\epsilon_{r, \text{trig}}$ in position components and $\epsilon_{v, \text{trig}}$ in velocity components

$$\|\mathbf{r}_0^N - \mathbf{r}_{N, \text{ref}}\|_2 \leq \epsilon_{r, \text{trig}}, \|\mathbf{v}_0^N - \mathbf{v}_{N, \text{ref}}\|_2 \leq \epsilon_{v, \text{trig}}. \quad (23)$$

Tolerances $\epsilon_{r, \text{trig}}$ and $\epsilon_{v, \text{trig}}$ do not need to be the same as ϵ_r and ϵ_v in (21). In fact, choosing $\epsilon_{r/v} < \epsilon_{r/v, \text{trig}}$ in general makes the closed loop more robust against uncertainties. When using (23), recursive feasibility may be recovered by considering the proof based on $\epsilon_{r, \text{trig}}$ and $\epsilon_{v, \text{trig}}$ instead of ϵ_r and ϵ_v , assuming a sufficiently large u_{max} .

V. NUMERICAL RESULTS

We conduct a Monte-Carlo experiment, where each sample consists of navigating and performing SK over 300 revolutions along the NRHO, corresponding to over 5.3 years. We use $K = 2$, $N = 6$, and $u_{\text{max}} = 1$ m/s, with triggering thresholds $\epsilon_{r, \text{trig}} = 100$ km and $\epsilon_{v, \text{trig}} = 20$ m/s, and terminal constraint radii $\epsilon_r = 25$ km and $\epsilon_v = 5$ m/s. All thresholds are defined in \mathcal{F}_{EM} . We conduct three separate experiments, using 1, 2, and 3 desaturation events per revolution, at θ_{desat} provided in Table I.

The dynamics is integrated using the explicit embedded Runge-Kutta Prince-Dormand (8,9) method from the GNU Scientific Library [22]. The SKMPC takes an average of 1.76 sec to solve on a single Intel i7-12700 CPU; the majority of the computational effort comes from propagating and constructing the STMs.

A. Navigation Performance

To assess the performance of the SKMPC, we first look at the navigation estimates provided to the controller. Figure 2 shows the estimation error of the EKF for the case involving

3 desaturation events; only the first 60 days are shown for the sake of clarity, as the filter performance is qualitatively similar across the remaining 240 days. The filter performance for 1 and 2 desaturation events are qualitatively similar. For assessing SK activities, we focus on navigation performance at the maneuver time. Table II shows the numerical $3\text{-}\sigma$ pre-maneuver state estimation error with 1, 2, and 3 desaturation events. As the number of desaturation events increases, the navigation error at the control epoch gets worse.

B. Cost Performance

The SK cost increases as the navigation performance worsens, as shown in Table III. Figure 3 shows the cumulative cost history with 3 desaturation events. Even in this case where the disturbance is largest, the cumulative cost follows a predominantly linear trend, indicating that the SKMPC is applying the appropriate level of control effort to keep the spacecraft motion near the baseline despite the uncertainties. Through preliminary experiments, we find the cumulative SK cost to be particularly sensitive to errors in velocity estimates. The costs reported in Table III are in accordance to our previous study [12] which assumed a fixed navigation uncertainty $3\text{-}\sigma$'s of 1.5 km and 0.8 cm/s, and is comparable to those reported with the use of the x -axis crossing control [2].

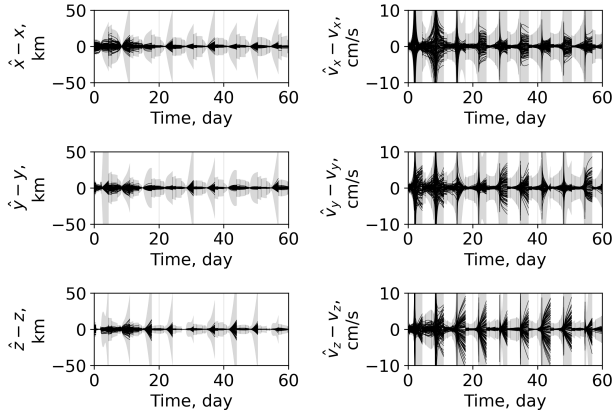


Fig. 2: Estimation error in \mathcal{F}_{Inn} with 3 desaturation events

TABLE II: Pre-maneuver state estimation error in \mathcal{F}_{EM}

Number of desaturation events	1	2	3
$(\hat{x} - x)$ $3\text{-}\sigma$, km	0.988	1.065	1.153
$(\hat{y} - y)$ $3\text{-}\sigma$, km	1.181	1.341	1.533
$(\hat{z} - z)$ $3\text{-}\sigma$, km	0.661	0.687	0.720
$(\hat{v}_x - v_x)$ $3\text{-}\sigma$, cm/s	0.199	0.206	0.213
$(\hat{v}_y - v_y)$ $3\text{-}\sigma$, cm/s	0.800	0.959	1.119
$(\hat{v}_z - v_z)$ $3\text{-}\sigma$, cm/s	0.110	0.122	0.138

C. Tracking Performance

We now analyze the tracking capability of the SKMPC. We first examine the deviation between the controlled spacecraft state and the baseline across the simulation horizon. We then look at the deviation of the epoch and state between the controlled spacecraft and the baseline.

TABLE III: Cost statistics from Monte-Carlo experiments

Number of desaturation events	1	2	3
Per maneuver mean, cm/s	2.42	2.95	3.69
Yearly mean, cm/s	120.63	162.58	196.12
Yearly standard deviation, cm/s	7.87	8.78	10.20
Yearly 95 th percentile, cm/s	133.32	177.52	213.11

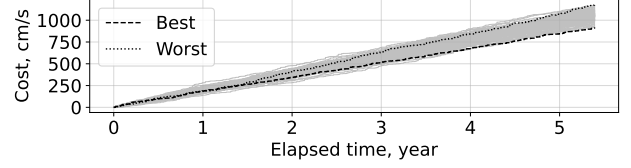


Fig. 3: Cumulative cost history with 3 desaturation events

1) *Global Tracking Performance*: Figure 4 shows the state deviation from the baseline over the first 60 days of the recursion. There is a clear periodic trend, where deviations are minimal except for the spikes at intervals of the NRHO period. These spikes correspond to perilune passes, where both the position and velocity vectors change rapidly. In such intervals, if there is a phase deviation, where the spacecraft leads ahead of or lags behind the baseline, the state deviation will be large even though the traced path itself may be close to the baseline.

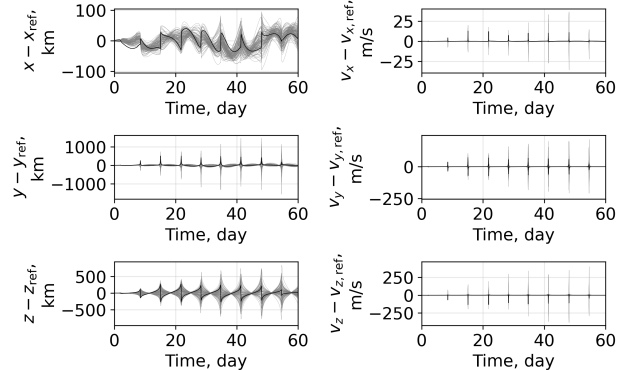


Fig. 4: State deviation in \mathcal{F}_{EM}

2) *Perilune Tracking Performance*: To isolate the effect of phase deviation, we compare the epochs and states at perilune passes to the corresponding perilune passes of the baseline. Figures 5 and 6 show the deviation of the epoch and state in \mathcal{F}_{EM} at each perilune passage. The SKMPC is found to keep the spacecraft to within 20 minutes of perilune pass deviation, with the pass occurring within position deviations of about 25 km and velocity deviations of about 5 m/s. In \mathcal{F}_{EM} , perilunes occur approximately along the $+z$ axis, with the spacecraft's motion approximately perpendicular to the position vector; thus, the error is found to be larger in z compared to x and y in position components, and v_x , and v_y compared to v_z in velocity components. The tracking performance is improved with the SKMPC compared to the x -axis crossing control which reports perilune deviations of up to 80 km in position and 48 minutes in epoch [2]; with

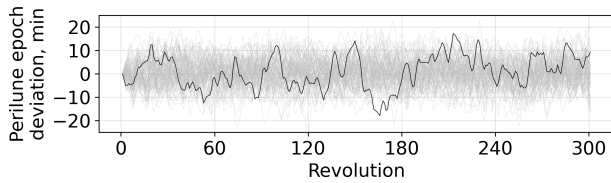


Fig. 5: Epoch deviation at perilune passes

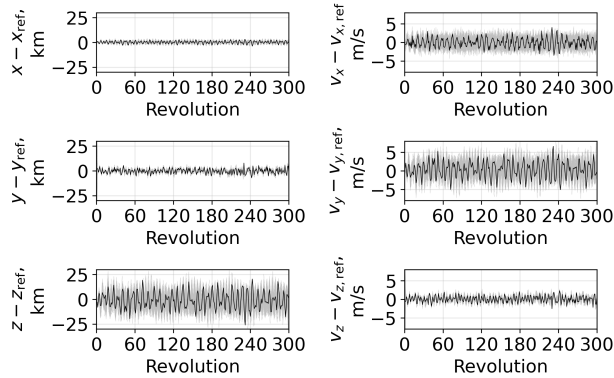


Fig. 6: State deviation in \mathcal{F}_{EM} at perilune passes

the SKMPC, we achieve a $3.2\times$ improvement in perilune position tracking, and a $2.4\times$ improvement in perilune epoch tracking. This improved tracking performance is due to the SKMPC avoiding phase drift through full-state tracking suffered by x -axis crossing control. In general, tighter tracking of the baseline is desirable since more stringent requirements can be met with regard to the spacecraft design or payload operations that require remaining closer to the intended path. For instance, the NRHO baseline for the Gateway is designed to be free of any Earth-shadowing eclipses [23], and tight tracking can ensure no such eclipse occurs during the flight subject to uncertainties as well.

VI. CONCLUSION

In this work, we proposed a targeting MPC for the SK problem on the NRHO. This SKMPC achieves full-state tracking by taking into account two maneuvers within its control horizon. The maneuvers are placed one revolution apart, making our approach compatible with the single maneuver-per-revolution requirement typical in space missions on the NRHO. Through full-state tracking, the SKMPC overcomes the issue of uncontrolled drift in phase ahead or behind the tracked baseline typically encountered by other state-of-the-art SK schemes with single maneuver-per-revolution. We demonstrated the SKMPC results in more precise tracking with output-feedback using an EKF with range and range-rate measurements, in closed loop with high-fidelity dynamics, and subject to realistic error models. Our approach achieves cumulative maneuver costs comparable to SK approaches proposed in the astrodynamics literature, while resulting in tighter tracking of the reference orbit in both space and phase without requiring additional ad-hoc heuristics, as in x -axis crossing control.

REFERENCES

- [1] D. E. Lee, "Gateway Destination Orbit Model: A Continuous 15 Year NRHO Reference Trajectory," NASA, Tech. Rep., 2019.
- [2] D. C. Davis, S. T. Scheuerle, D. A. Williams, F. S. Miguel, E. M. Zimovan-Spreen, and K. C. Howell, "Orbit Maintenance Burn Details for Spacecraft in a Near Rectilinear Halo Orbit," in *AAS/AIAA Astrodynamics Specialists Conference*, 2022.
- [3] B. Cheetham, T. Gardner, A. Forsman, E. Kayser, and M. Clarkson, "CAPSTONE: A Unique CubeSat Platform for a Navigation Demonstration in Cislunar Space," in *ASCEND 2022*. Reston, Virginia: American Institute of Aeronautics and Astronautics, 2022, pp. 1–10.
- [4] D. A. P. Williams, K. C. Howell, and D. C. Davis, "A Comparison of Station-Keeping Strategies for Halo Orbits," in *AAS/AIAA Astrodynamics Specialist Conference*, vol. 231, 2023, pp. 1–20.
- [5] Y. Shimane, K. Ho, and A. Weiss, "Optimization-Based Phase-Constrained Station-Keeping Control on Libration Point Orbit," in *AAS/AIAA Astrodynamics Specialists Conference*, 2024, pp. 1–19.
- [6] M. Shirobokov, S. Trofimov, and M. Ovchinnikov, "Survey of station-keeping techniques for libration point orbits," *Journal of Guidance, Control, and Dynamics*, vol. 40, no. 5, pp. 1085–1105, 2017.
- [7] J. B. Rawlings, D. Angeli, and C. N. Bates, "Fundamentals of economic model predictive control," *Proceedings of the IEEE Conference on Decision and Control*, pp. 3851–3861, 2012.
- [8] D. Angeli, "Economic Model Predictive Control," in *Encyclopedia of Systems and Control*, J. Baillieul and T. Samad, Eds. London: Springer London, 2015.
- [9] G. Misra, H. Peng, and X. Bai, "Halo orbit station-keeping using nonlinear MPC and polynomial optimization," in *AAS/AIAA Space Flight Mech. Meeting*, 2018.
- [10] P. Elango, S. Di Cairano, U. Kalabic, and A. Weiss, "Local Eigenmotion Control for Near Rectilinear Halo Orbits," in *Proceedings of the American Control Conference*, vol. 2022-June, 2022, pp. 1822–1827.
- [11] R. Padhi, A. Banerjee, S. Mathavaraj, and V. Srikanth, "Computational Guidance Using Model Predictive Static Programming for Challenging Space Missions: An Introductory Tutorial with Example Scenarios," *IEEE Control Systems*, vol. 44, no. 2, pp. 55–80, 2024.
- [12] Y. Shimane, S. Di Cairano, K. Ho, and A. Weiss, "Station-Keeping on Near-Rectilinear Halo Orbits via Full-State Targeting Model Predictive Control," in *American Control Conference*, 2025 (submitted).
- [13] W. McClain and D. Vallado, *Fundamentals of Astrodynamics and Applications*, ser. Space Technology Library. Springer Netherlands, 2001.
- [14] C. Acton, N. Bachman, B. Semenov, and E. Wright, "A look towards the future in the handling of space science mission geometry," *Planetary and Space Science*, vol. 150, no. January 2017, pp. 9–12, 2018.
- [15] E. M. Zimovan-Spreen, K. C. Howell, and D. C. Davis, "Dynamical Structures Nearby NRHOs with Applications to Transfer Design in Cislunar Space," *Journal of the Astronautical Sciences*, vol. 69, no. 3, pp. 718–744, jun 2022.
- [16] J. R. Carpenter and C. N. D'souza, "Navigation Filter Best Practices," NASA Engineering and Safety Center, Tech. Rep. TP-2018-219822 Navigation, 2018.
- [17] P. Elango, S. Di Cairano, K. Berntorp, and A. Weiss, "Sequential linearization-based station keeping with optical navigation for NRHO," in *AAS/AIAA Astrodynamics Specialist Conference*, 2022.
- [18] A. Domahidi, E. Chu, and S. Boyd, "ECOS: An SOCP solver for embedded systems," in *European Control Conference (ECC)*, 2013, pp. 3071–3076.
- [19] B. O'Donoghue, E. Chu, N. Parikh, and S. Boyd, "Conic optimization via operator splitting and homogeneous self-dual embedding," *Journal of Optimization Theory and Applications*, vol. 169, no. 3, pp. 1042–1068, June 2016.
- [20] C. R. Gates, "A Simplified Model of Midcourse Maneuver Execution Errors," Jet Propulsion Laboratory, Tech. Rep., 1963.
- [21] M. Bolliger, M. R. Thompson, N. P. Ré, C. Ott, and D. C. Davis, "Ground-Based Navigation Trades for Operations in Gateway's Near Rectilinear Halo Orbit," in *AAS/AIAA Space Flight Mechanics Meeting*, 2021.
- [22] B. Gough, *GNU scientific library reference manual*. Network Theory Ltd., 2009.
- [23] E. M. Zimovan-spreen, S. T. Scheuerle, B. P. McCarthy, D. C. Davis, and K. C. Howell, "Baseline Orbit Generation For Near Rectilinear Halo Orbits," in *AAS/AIAA Astrodynamics Specialist Conference*, 2023, pp. 1–20.